Excitation Energy Transfer in Photosynthetic Pigment-Protein Complexes and Membrane Models

CLOSING REPORT

Preface

In this project, we investigated the dynamics of excitation energy transfer (EET) in photosynthetic pigment-protein complexes (PPCs) and the role of molecular interactions therein. The scientific results obtained in the course of the project contribute to our understanding of the pathways and dynamics of EET in light-harvesting complex II (LHCII), Photosystem II (PSII) and Photosystem I (PSI), in the cyanobacterial phycobilisomes (PBSs) and between the PBSs and the photosystems. We used novel methodological approaches to reconstitute LHCII in lipid membranes for single-molecule studies and for an accurate determination of the dependence of the excited-state lifetime on the lipid:protein (L/P) ratio, demonstrating the intrinsic capacity of LHCII for photoprotective non-photochemical quenching. The mechanisms and dynamics of photobleaching of LHCII in detergent and lipid environments were compared and the inherent susceptibility of the lipid membrane to photosensitized oxidative damage was revealed.

The scientific results were presented at numerous international conferences and were published in **17 research articles in peer-reviewed scientific journals, two invited review articles and one book chapter**. All articles were published in journals ranked in the **first quartile** (by SJR or JCR), with a **cumulative impact factor of 69** (using the journal IF up to the year 2019). **Six joint articles** were co-authored by the main international partner.

In the following, we will summarize the main scientific results grouped according to the two key goals in the research proposal.

1 Dynamics of excitation energy transfer in the photosynthetic membranes

1.1 Ultrafast excitation dynamics in LHCII

EET in LHCII was investigated by two-dimensional electronic spectroscopy (2DES) at different temperatures from 77 to 295 K (1). The experiments were performed using broadband excitation pulses covering most of the chlorophyll (Chl) Q_y region and under conditions free from singlet-singlet annihilation. The results showed that EET between Chls slows down as temperature is lowered, in part due to blocking of energetically uphill pathways. The EET lifetimes showed considerable temperature dependence – the slowest timescale of equilibration with the lowest-energy Chl *a* increased from ~5 ps at 295 K to ~15 ps at 77 K (Fig. 1). At temperatures above protein glass transition, the final excited state was independent of the excitation wavelength, whereas static energy disorder became apparent at lower temperatures. A clear temperature dependence of uphill EET processes was also discerned – cross-peaks in the 2D electronic spectra reflecting the population uphill transfer (from lower- to higher-energy states) diminished with lowering the temperature (Fig. 1), consistent with the detailed-balance condition. The 2D electronic spectra recorded at 77 K revealed a wealth of information about the pathways of EET and served as a basis for phenomenological modelling of the excitation dynamics (2). By fitting the model parameters to the experimental 2D electronic spectra, the phenomenological modelling procedure

recovered the excitonic energy levels, dipole strength, homogeneous and inhomogeneous linewidths, and EET rates between states. Although it was not possible to determine all EET rates uniquely, a recurring pattern of EET with very similar overall timescales between spectral components (excitons) was consistently obtained. Tentative pigment assignment based on the interpretation of the modelling results together with previous structure-based calculations and spectroscopic observables were was proposed. These results were discussed in a broader context in a review article (3).

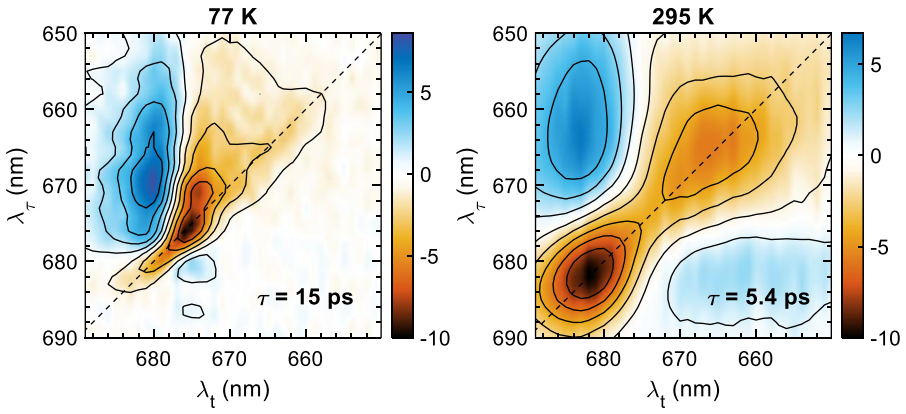

Fig. 1. Comparison of slower energy transfer 2D decay-associated spectra of LHCII at 77 K and 295 K. Red/blue colours represent negative/positive amplitudes (decay/rise of the negative absorptive signal)

To shed more light onto the temperature dependence of the EET dynamics of LHCII, 2D electronic spectra were calculated for different temperatures using non-perturbative quantum-mechanical theory (4). The simulations provided theoretical confirmation for the assignments of uphill and downhill EET processes, observed as 2D spectral features. The calculated transfer rates at room temperature were very similar to the measured rates. Deviations in certain rates indicate that the model Hamiltonian used needs refinement. Larger discord between the theory and experiment was found for low temperatures, which indicates that the temperature dependence of the model parameters is not fully described by the state-of-art theories.

The EET dynamics in LHCII monomerized by phospholipase treatment was also investigated by 2DES at room temperature and 77 K. The 2DES results at room temperature showed that spectral equilibration occurs predominantly within the monomeric subunits. However, marked differences were observed in the kinetics at 77K. Exciton relaxation was slower in monomers; for instance, the transfer from Chl *a* absorbing at 670 nm to the lowest-energy state slowed down by more than 50%. Moreover, the 2D peaks in monomers were more inhomogeneously broadened indicating higher degree of structural disorder. These results suggest that that the trimeric organization of LHCII has structure-stabilizing role.

1.2 Spectral tuning of LHCII in the green alga *Bryopsis corticulans*

LHCII from the marine siphonous green macroalga *Bryopsis corticulans* was spectroscopically characterized to understand the structural and functional changes resulting from adaptation to intertidal environment (5). LHCII from *B. corticulans* is homologous to the PSII antenna of land plants but has a different carotenoid and Chl composition to optimize the absorption of blue-green light. To assess how this adaptive change in the pigment composition of LHCII affects the spectroscopic and dynamic properties, we measured steady state absorption, fluorescence, circular and anisotropic circular dichroism (CD and ACD) spectra. Compared to higher-plant LHCII, the complex contains two additional spectral forms of Chl *b* – absorbing at around 650 nm and 658 nm, at the expense of Chl *a* absorbing around 674 nm and 679 nm – the lowest-energy Chl a form. The distinctive ACD signature assigned to the lowest-energy Chl a in higher plants (6) was absent in the spectra of *B. corticulans* indicating the

replacement of lowest-energy state of plants. 2DES of LHCII from *B. corticulans* showed the existence of long-lived Chl *b* that is weakly coupled to Chl *a* (Fig. 2) and slower exciton equilibration in the Chl a manifold compared to higher plants. In other words, there is a tradeoff between the increased absorption cross-section at shorter wavelengths and the excitation migration time, which however does not negatively impact the photosynthetic efficiency. These results show that LHCII is a robust and tuneable system that can be adapted to the light environment while maintaining efficiency.

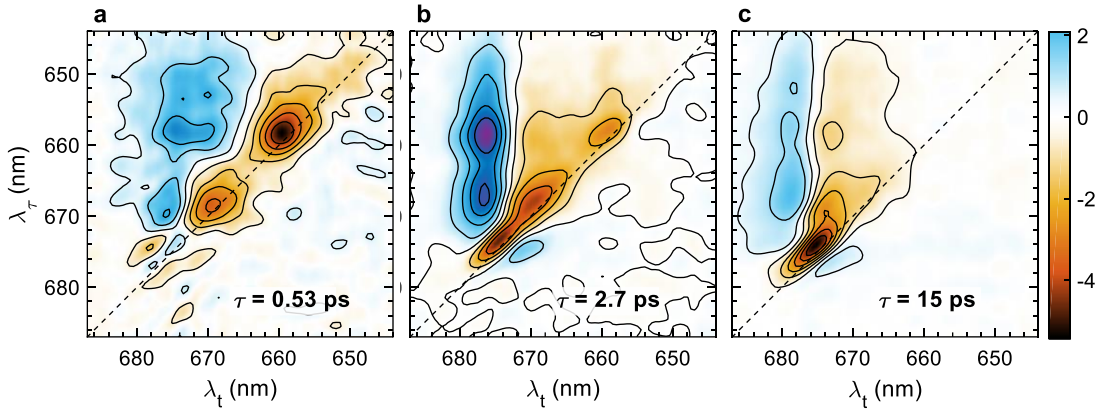

Fig. 2. 2D decay-associated spectra of LHCII at 77 K, obtained from four-component global lifetime analysis of the 2D electronic spectra. Red/blue colours represent negative/positive amplitudes (decay/rise of the negative absorptive signal). The final component representing decay to the ground state is omitted.

Phenomenological model fitting was applied to extract information about the excitonic states and EET processes in LHCII from *B. corticulans* (7). The fitting method results in well converged parameters, including excitonic energy levels with their respective transition dipole moments, spectral widths, EET rates and coupling properties. The 2D spectra simulated from the fitted parameters concur very well with the experimental data, showing the robustness of the fitting method. An excitonic EET scheme was proposed based on the fitting parameters. In addition to other details, three weakly-connected terminal states were resolved at 671, 675 and 677 nm and the lowest state was higher in energy than that in plant LHCII, which is probably because of the fewer number of Chls *a* in a *B. corticulans* LHCII monomer. Several possible Chl *a*–*b* replacements were suggested based on the modeling based on existing Hamiltonians for the plant LHCII structure with two Chls *a* switched to Chls *b*.

1.3 Dynamics of energy transfer in photosystem I at 77 K

PSI of almost all organisms contains a number of long-wavelength-absorbing Chl forms, dubbed "red" Chls, absorbing light at wavelengths longer than the absorption of the reaction centre (RC) Chls. We quantified the red forms in plant PSI and clarified their spectroscopic characteristics, which have profound implication on understanding the EET and charge separation dynamics (8). We compared the steady-state absorption and fluorescence spectra and picosecond time-resolved fluorescence kinetics of isolated PSI core complex and PSI–LHCI supercomplex from *Pisum sativum* recorded at 77 K. We found that the core complex contains "red" Chls with absorption at around 705 nm with an oscillator strength of three Chls. The peripheral antenna in PSI–LHCI contained up to five red Chls with absorption at 703 nm and 711 nm. From the fluorescence emission spectra, we could identify states emitting at different wavelengths in the core and LHCI. The red states compete with the reaction centre (P_{700}) in trapping excitations in the bulk antenna, which occurs on a timescale of ~20 ps. The three red forms in the core have distinct decay kinetics (Fig. 3), probably in part determined by the rate of quenching by the oxidized P_{700}. These results confirm that the red Chls in the core complex must not be neglected when interpreting kinetic experimental results of PSI.

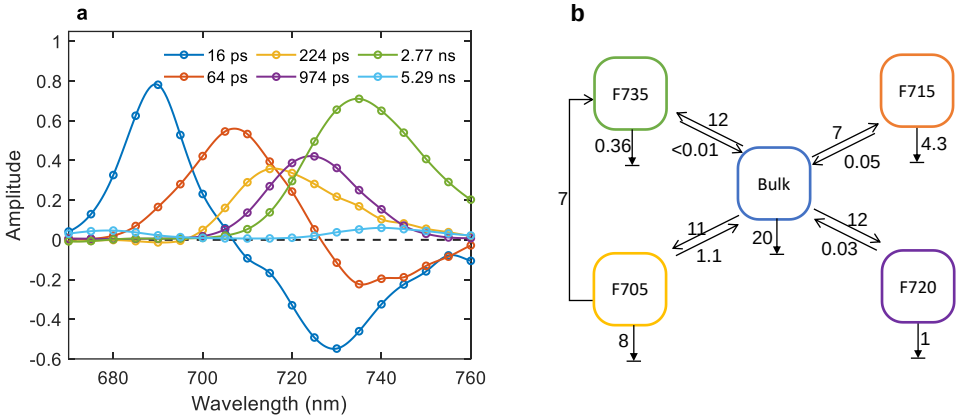

Fig. 3. EET to the red Chls in plant PSI-LHCI complexes at 77 K: a) decay-associated fluorescence emission spectra; b) EET scheme resulting from kinetic modelling of the time-resolved fluorescence data.

We investigated the pigment spectral forms, especially for red Chls, in monomers and trimers of Photosystem I from *Synechocystis* PCC 6803 (9). We compared the absorption, emission, and CD spectra of the trimeric PSI with a monomeric complex isolated from the Δ*psaL* strain, and a subunit-depleted monomeric complex ΔFIJL, containing only subunits A, B, C, D, E, K and M. The monomeric complexes had a reduced far-red absorption and emission equivalent to the loss of 1.5–2 red Chls emitting at 710–715 nm, whereas the longest-wavelength emission at 722 nm was not affected. The quantum yield of photochemistry at room temperature was the same in all complexes, demonstrating the functional robustness of this photosystem. Time-resolved fluorescence spectroscopy at 77 K resolved spectrally and kinetically distinct pools of red Chls in all complexes and equilibration times of up to 50 ps (Fig. 4). Monomeric complexes had markedly different kinetics in the far-red region. To explain this, we hypothesized that intermediate-energy red Chls at the monomer interface (assigned to Chl A32/B7) facilitate energy migration from the lowest-energy states to the RC.

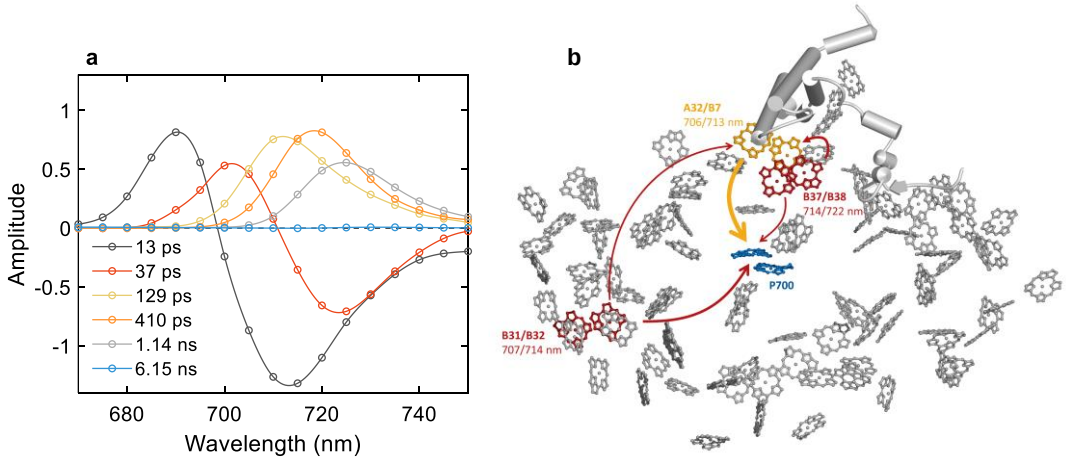

Fig. 4. EET to the red Chls in PSI from *Synechocystis* at 77 K: a) decay-associated fluorescence emission spectra of trimeric PSI b) schematic structure of PSI (one monomer) showing uphill EET from the assigned red Chls to P_{700}.

1.4 Excitation dynamics in dark- and light-adapted Photosystem II

A growing body of evidence has emerged that the variable fluorescence of Photosystem II (PSII), i.e. the rise of the fluorescence yield from F_o, in a dark-adapted state, to F_m, after illumination with saturating light, does not reflect solely the photochemical reduction of the electron acceptor Q_A (10). We measured the picosecond fluorescence decay kinetics of isolated PSII cores at room temperature and 278 K in three different states: dark-adapted open state ($PSII_O$), dark-adapted closed state, induced by preillumination

with a single-turnover saturating flash ($PSII_C$) and light-adapted closed state ($PSII_L$) (11). The fluorescence decay lifetimes in $PSII_O$ and $PSII_L$ reproduced published data from other groups. The average fluorescence lifetime increased more than 5-fold in $PSII_L$, as does the fluorescence yield – rising from F_o to F_m. On the other hand, fully reducing Q_A by a single-turnover flash resulted in only a moderate change in the fluorescence kinetics, increasing the average lifetime from 110 ps to about 220 ps. Additional flashes further slowed down the fluorescence decay kinetics. These results unambiguously confirm that the maximal fluorescence yield of PSII cannot be achieved by reducing Q_A alone. The fluorescence intensity increment observed during the transition from $PSII_C$ to $PSII_L$ is associated with changes in the Chl excited-state dynamics in the PSII core. Conversely, the data reveal the presence of an efficient de-excitation channel in $PSII_C$, most likely nonradiative recombination of transiently generated radical pairs. In support of this interpretation, kinetic model fitting of the time-resolved fluorescence data showed that the free-energy gap of the secondary radical pairs decreases upon $PSII_C$–$PSII_L$ transition, shifting the exciton-radical pair equilibrium (Fig. 5). These results reaffirm the functional separation of the dark- and light-adapted closed state of PSII, and the role of structural dynamics of PSII in the transitions between them.

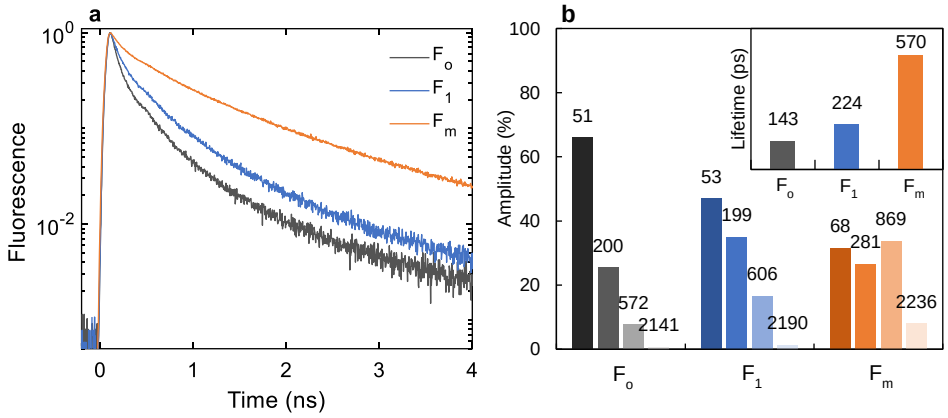

Fig. 5. Fluorescence decay kinetics of PSII under $PSII_O$ (F_o), $PSII_C$ (F_1) and $PSII_L$ (F_m) conditions. (a): Fluorescence decays recorded at 685 nm; (b): distribution of fluorescence lifetime components by their relative amplitudes.

1.5 Energy transfer in phycobilisomes and between phycobilisomes and photosystems in cyanobacteria

We studied the dynamics of EET in the whole cells of the cyanobacteria *Synechocystis* PCC 6803 and *Anabaena* PCC 7120 as well as in isolated PBSs and photosystem complexes (12). We found that the photochemical rate of the tetrameric PSI of *Anabaena* is slower (40 ps) compared to *Synechocystis*, likely related to the higher number of long-wavelength antenna Chls. The equilibration time with the long-wavelength forms was found to be 10–15 ps. We could resolve EET steps between the phycocyanin rods and from the rods to allophycocyanin core, both in isolated PBS and in whole cells. Despite specifics in the PBS composition (containing phycoerythrin) and architecture (having a pentameric core), the kinetics of energy transfer and trapping in Anabaena was found to be remarkably similar to Synechocystis. Simultaneous kinetic modelling of the fluorescence decays of whole cells and isolated complexes was developed to resolve the rates of EET (13). According to the model, the rate-limiting step in vivo is EET from the phycocyanin rods to the allophycocyanin core of the PBS. Fast EET from the terminal allophycocyanin in the PBS core to Chl *a* in both PSI and PSII suggests strong energetic coupling between the soluble PBS and the membrane-bound photosystems.

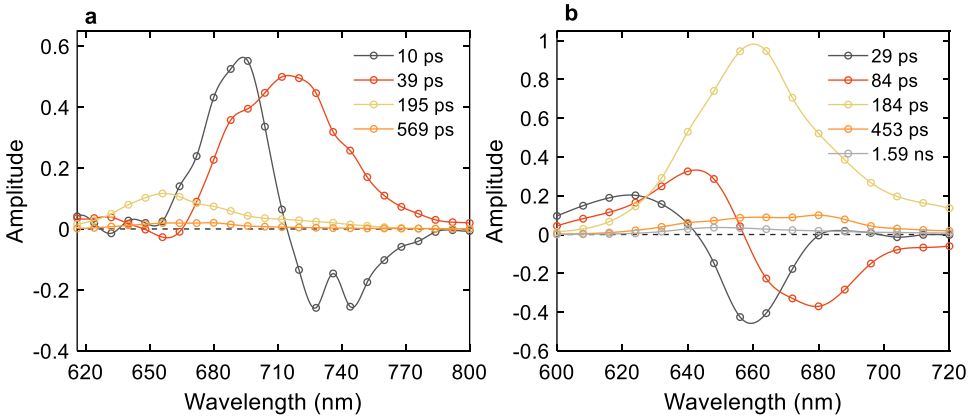

Fig. 6. Decay-associated fluorescence emission spectra of whole cells of *Anabaena variabilis*. (a): selective excitations of Chl at 460 nm; (b): selective excitations of PBS at 580 nm.

Filamentous cyanobacteria like *Anabaena*, when experiencing nitrogen nutrient deficiency, can form nitrogen-fixating heterocyst cells. In heterocysts, the phycobiliproteins and PSII are gradually degraded but a functional PSI is retained. We isolated heterocysts from nitrogen-depleted *Anabaena* cultures and investigated the excitation dynamics using time-resolved fluorescence spectroscopy. Heterocysts exhibited drastically different dynamics compared to vegetative cells. The fluorescence kinetics may reflect EET from phycocyanin in a PBS–PSI supercomplex. However, the data were marred by long-lived decay components possibly from cell debris. To avoid this contamination, the fluorescence lifetime imaging technique was used (in collaboration with Dr. Emilie Wientjes, Wageningen University, Netherlands). In this way fluorescence kinetics could be recorded from single heterocysts and direct EET from phycocyanin to PSI was confirmed.

2 Molecular interaction effects on the excited states and dynamics of LHCII

2.1 Identifying exciton states in LHCII by anisotropic circular dichroism

Anisotropic CD (ACD) is capable of distinguishing between optical transitions having different orientations with respect to the molecular frame (14). We incorporated LHCII into lipid vesicles to facilitate macroscopic orientation of the complexes and measured ACD spectra in the visible as well as the far- and near-UV regions (6). The ACD spectra showed drastically enhanced magnitude and level of detail compared to the corresponding isotropic CD spectra, resolving a greater number of bands and revealing transitions that were too weak to be resolved in absorption and CD spectra. A striking sign-inversion of the red-most band of the CD spectrum, originating from the lowest-energy excitonic states, was demonstrated. Theoretical calculations performed in collaboration with Prof. Thomas Renger and coworkers showed that the spectral features in the Chl Q_y region were well reproduced by an existing excitonic model for LHCII providing evidence for the identity of the Chls forming the lowest-energy states.

2.2 Heterogeneity of reconstituted LHCII model membranes

Incorporation of membrane proteins into reconstituted lipid membranes is a common approach for studying their structure and function in a native-like environment. Using lipophilic fluorescent dyes (DiI), we were able to estimate the actual lipid:protein ratios of reconstituted LHCII proteoliposomes. Single-molecule microscopy was further employed to quantify the vesicle size, curvature and the lipid and protein content of individual proteoliposomes (15). Proteoliposomes displayed a high degree of

heterogeneity with respect to size, protein density and fluorescence yield (Fig. 7). The vesicles of larger size appeared to have few proteins compared to smaller vesicles. These experiments showed quantitatively that the liposome formation and subsequent reconstitution of the LHCII complexes into them result in by-all-means heterogeneous systems with individual properties largely differing from the ensemble average. Further, by using time-resolved fluorescence, we found a strong correlation between the fluorescence quenching and the lipid:protein ratio (16). The results clearly demonstrate that the fluorescence yield and the fluorescence lifetime are gradually reduced with increasing protein density to values comparable with those of strongly-quenched aggregates. Moreover, we showed that the onset of quenching is correlated with the appearance of far-red fluorescence emission, which had been previously observed both in artificial aggregates and in intact plant leaves under NPQ conditions. Thus, our results demonstrated that NPQ can be induced by LHCII-LHCII interactions in reconstituted membranes, most likely occurring via the same mechanism as photoprotective NPQ in vivo. Single-liposome microscopic fluorescence lifetime measurements confirmed the confirmed that the fluorescence quenching of LHCII was inversely correlated with the lipid:protein ratio (17).

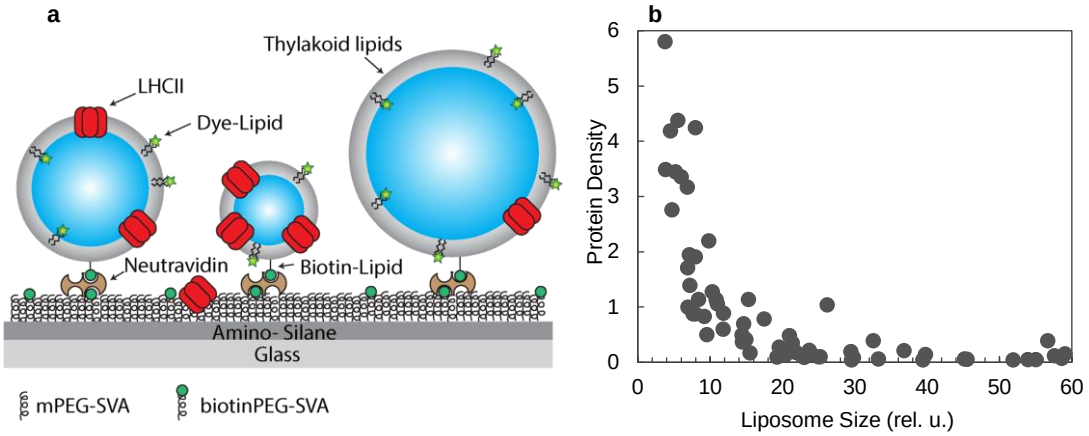

Fig. 7. LHCII proteoliposomes with different lipid:protein ratios and their size and fluorescence lifetimes: a) illustration of liposomes with LHCII and lipid dyes immobilized on a glass surface for microscopic measurements; b) dependence of the protein density (number of LHCII per area) as function of the lipid:protein ratio in single proteoliposomes.

2.3 Spectroscopic studies on LHCII crystals

In collaboration with Dr. Mei Li (Institute of Biophysics, Chinese Academy of Sciences, Beijing), we measured the optical spectra and excitation dynamics of membrane crystals of LHCII with known X-ray crystallographic structure. The size and geometry of the crystals largely determine whether they can be analysed by various spectroscopic techniques. Thin microcrystals can be subjected to optical measurements in transmission mode. Bulk CD spectra recorded from the crystals in suspension showed that the CD spectra of such crystals are different compared to the CD spectra of LHCII trimers in detergent micelles (Fig. 8). Remarkably, the crystal CD spectra were strongly reminiscent of LHCII monomers in solution, although the X-ray structure clearly shows the trimeric organization of the crystallized complexes. We recorded synchrotron-radiation CD spectra from single crystals using highly collimated microbeam at the Diamond synchrotron (UK). To this end, crystal suspension was deposited on a window and placed on a motorized X-Y scanning stage. CD spectra were then recorded from a 1x1 mm area with 100 µm spatial resolution. The UV region of crystals and solubilized trimers showed no significant differences. However, the crystals exhibited markedly different CD in the visible region, especially between 450 and 500 nm, confirming the bulk measurements. The crystal spectra closely resemble the CD spectra of oriented LHCII membranes. Further, we obtained time-resolved fluorescence data of single crystals by fluorescence lifetime imaging and time-resolved fluorescence. The fluorescence

lifetime of the crystals was significantly shorter (up to 4x) than in detergent and the decays were multiexponential. The induced fluorescence quenching in the crystals agrees with the postulation that LHCII has the intrinsic capability of fluorescence quenching that is activated whenever the complexes form densely packed domains.

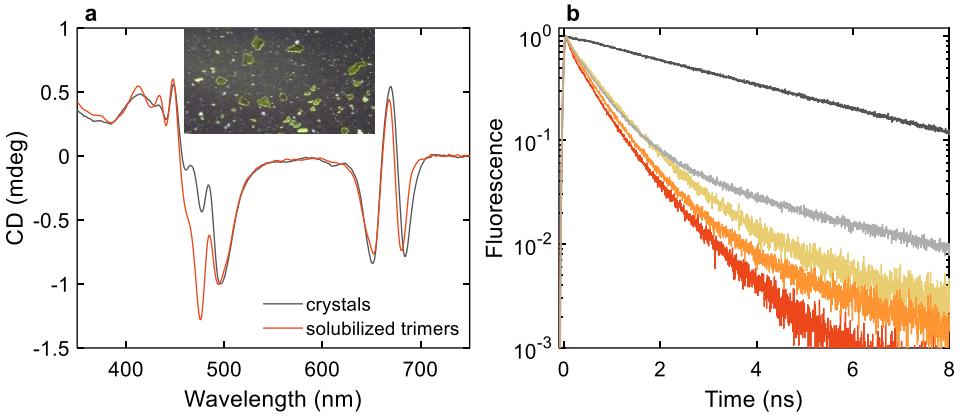

Fig. 8. Spectroscopy of LHCII crystals: a) CD spectra of LHCII crystals compared with solubilised LHCII trimers (inset: light microscope image of LHCII crystals); b) Fluorescence decay curves of crystals collected from different crystallization wells and compared with LHCII trimers (gray curve). The emission was measured at 680 nm with excitation at 633 nm.

2.4 Mechanism of non-photochemical quenching in LHCII aggregates and crystals

The fluorescence decay kinetics of LHCII crystals and aggregates recorded with picosecond resolution at temperatures down to 4 K were analysed (18). The fluorescence kinetics of aggregates and crystals and their wavelength and temperature dependence were similar and starkly different from detergent-solubilized (unquenched) LHCII. Both crystals and aggregates showed strong far-red emission attributed to the formation of weakly emitting Chl–Chl charge transfer (CT) states. Kinetic modelling of the data showed that these states are an intrinsic part of the fluorescence quenching despite the fact that they are generally longer-lived than the bulk Chl excited states. Quantum chemical calculations of the lowest energy exciton and CT states, explicitly including the coupling to the specific protein environment, provided detailed insight into the chemical nature and mechanism of CT quenching. The experimental data combined with the results of the calculations strongly suggest that the quenching mechanism involves electron transfer steps between the lowest-energy Chls, and that it is switched by polarity-controlled internal reprotonation of neighbouring protein residues. A unified model was thus proposed able to explain fluorescence quenching in LHCII depending on the environment without invoking major conformational changes of the protein.

2.5 Mechanisms of photodamage of LHCII in reconstituted membranes

We evaluated the susceptibility of isolated LHCII to photodamage and its dependence on the molecular environment (19). The light-dependent bleaching of LHCII in different molecular environments (LHCII solubilized in detergent, aggregates, reconstituted LHCII membranes) was quantified spectroscopically. LHCII in reconstituted lipid membranes was found substantially more susceptible to photodegradation compared to detergent-solubilized or aggregated complexes (Fig. 9). The process was strongly oxygen-dependent and the rate of photodegradation was lower in anoxic environment as well as in the presence of ascorbate added as an antioxidant. Malondialdehyde-thiobarbituric acid reactivity test indicated light-induced peroxidation of membrane lipids. The increased production of singlet oxygen in the light-exposed LHCII was confirmed by electron paramagnetic resonance (EPR) spectroscopy using spin traps and spin labels (Fig. 9). The quantum yield of Chl *a* photobleaching in membranes and detergent was found to be 3.4×10^{-5} and 1.4×10^{-5}, respectively. These values suggest that direct photodamage of the

antenna occurs with rates relevant to photoinhibition *in vivo*. The results represent further evidence that the molecular environment of LHCII has profound impact on its functional characteristics, including, among others, the susceptibility to photodamage.

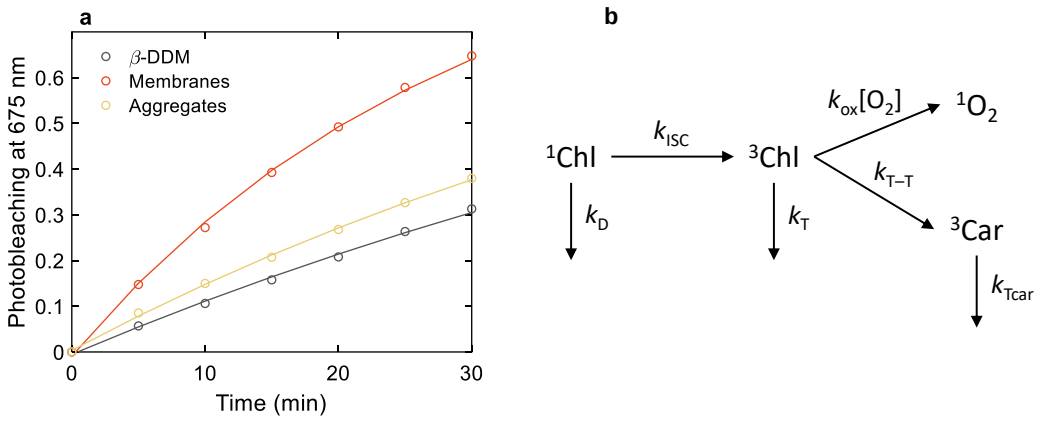

Fig. 9. Photobleaching of LHCII in different molecular environments: a) Time course of photobleaching of LHCII in detergent (β-DDM), reconstituted membranes and aggregates during 30 min of irradiation (2000 mmol photons m^{-2} s^{-1}); b) Kinetic scheme of photobleaching by the sensitization of singlet oxygen (k_D = 0.2 ns^{-1}, k_{ISC} = 0.1 ns^{-1}, k_T = 1 ms^{-1}, 1 ms^{-1}, k_{T-T} = 2 ns^{-1}, k_{ox} = 2 M^{-1} ns^{-1}).

Publications

1. Akhtar P, Do TN, Nowakowski PJ, Huerta-Viga A, Khyasudeen MF, Lambrev PH, et al. Temperature dependence of the energy transfer in LHCII revealed by two-dimensional electronic spectroscopy. J Phys Chem B. 2019;123(31):6765–75. doi.org/10.1021/acs.jpcb.9b05421.
2. Do TN, Huerta-Viga A, Akhtar P, Nguyen HL, Nowakowski PJ, Khyasudeen MF, et al. Revealing the excitation energy transfer network of Light-Harvesting Complex II by a phenomenological analysis of two-dimensional electronic spectra at 77 K. J Chem Phys. 2019;151(20):205101. doi.org/10.1063/1.5125744.
3. Lambrev PH, Akhtar P, Tan H-S. Insights into the mechanisms and dynamics of energy transfer in plant light-harvesting complexes from two-dimensional electronic spectroscopy. Biochim Biophys Acta. 2020;1861(4):148050. doi.org/10.1016/j.bbabio.2019.07.005.
4. Leng X, Do TN, Akhtar P, Nguyen HL, Lambrev P, Tan HS. Hierarchical equations of motion simulation of temperature-dependent two-dimensional electronic spectroscopy of the chlorophyll *a* manifold in LHCII. Chemistry—An Asian Journal. 2020;15(13):1996–2004. doi.org/10.1002/asia.202000467.
5. Akhtar P, Nowakowski PJ, Wang W, Do TN, Zhao S, Siligardi G, et al. Spectral tuning of light-harvesting complex II in the siphonous alga Bryopsis corticulans and its effect on energy transfer dynamics. Biochim Biophys Acta Bioenerg. 2020;1861(7):148191. 10.1016/j.bbabio.2020.148191.
6. Akhtar P, Lindorfer D, Lingvay M, Pawlak K, Zsiros O, Siligardi G, et al. Anisotropic circular dichroism of light-harvesting complex II in oriented lipid bilayers: Theory meets experiment. J Phys Chem B. 2019;123(5):1090–8. doi.org/10.1021/acs.jpcb.8b12474.
7. Nguyen HL, Do TN, Akhtar P, Jansen TL, Knoester J, Wang W, et al. An Exciton Dynamics Model of Bryopsis corticulans Light-Harvesting Complex II. J Phys Chem B. 2021;125(4):1134–43. doi.org/10.1021/acs.jpcb.0c10634.
8. Akhtar P, Lambrev PH. On the spectral properties and excitation dynamics of long-wavelength chlorophylls in higher-plant photosystem I. Biochim Biophys Acta. 2020;1861(11):148274. doi.org/10.1016/j.bbabio.2020.148274.
9. Akhtar P, Biswas A, Kovács L, Nelson N, Lambrev PH. Excitation energy transfer kinetics of trimeric, monomeric and subunit-depleted Photosystem I from Synechocystis PCC 6803. Biochem J. 2021 doi.org/10.1042/BCJ20210021.
10. Sipka G, Muller P, Brettel K, Magyar M, Kovacs L, Zhu Q, et al. Redox transients of P680 associated with the incremental chlorophyll-a fluorescence yield rises elicited by a series of saturating flashes in diuron-treated Photosystem II core complex of Thermosynechococcus vulcanus. Physiol Plant. 2019;166(1):22–32. doi.org/10.1111/ppl.12945.
11. Sipka G, Magyar M, Mezzetti A, Akhtar P, Zhu Q, Xiao Y, et al. Light-Adapted Charge-Separated State of Photosystem II: Structural and Functional Dynamics of the Closed Reaction Center. Plant Cell. 2021 doi.org/10.1093/plcell/koab008.
12. Akhtar P, Biswas A, Petrova N, Zakar T, van Stokkum IHM, Lambrev PH. Time-resolved fluorescence study of excitation energy transfer in the cyanobacterium Anabaena PCC 7120. Photosynth Res. 2020;144(2):247–59. doi.org/10.1007/s11120-020-00719-w.
13. Biswas A, Huang X, Lambrev PH, van Stokkum IH. Modelling excitation energy transfer and trapping in the filamentous cyanobacterium *Anabaena variabilis* PCC 7120. Photosynth Res. 2020;144(2):261–72. doi.org/10.1007/s11120-020-00723-0.
14. Lambrev PH, Akhtar P. Macroorganisation and flexibility of thylakoid membranes. Biochem J. 2019;476(20):2981–3018. doi.org/doi.org/10.1042/bcj20190080.

15. Tutkus M, Akhtar P, Chmeliov J, Görföl F, Trinkunas G, Lambrev PH, et al. Fluorescence microscopy of single liposomes with incorporated pigment–proteins. Langmuir. 2018;34(47):14410–8. doi.org/10.1021/acs.langmuir.8b02307.
16. Akhtar P, Görföl F, Garab G, Lambrev PH. Dependence of chlorophyll fluorescence quenching on the lipid-to-protein ratio in reconstituted light-harvesting complex II membranes containing lipid labels. Chem Phys. 2019;522:242–8. doi.org/10.1016/j.chemphys.2019.03.012.
17. Tutkus M, Chmeliov J, Trinkunas G, Akhtar P, Lambrev PH, Valkunas L. Aggregation-related quenching of LHCII fluorescence in liposomes revealed by single-molecule spectroscopy. J Photochem Photobiol B: Biol. 2021:112174. doi.org/10.1016/j.jphotobiol.2021.112174.
18. Ostroumov EE, Götze JP, Reus M, Lambrev PH, Holzwarth AR. Characterization of fluorescent chlorophyll charge-transfer states as intermediates in the excited state quenching of light-harvesting complex II. Photosynth Res. 2020;144(2):171–93 doi.org/10.1007/s11120-020-00745-8.
19. Lingvay M, Akhtar P, Sebők-Nagy K, Páli T, Lambrev PH. Photobleaching of Chlorophyll in Light-Harvesting Complex II Increases in Lipid Environment. Front Plant Sci. 2020;11:849. doi.org/10.3389/fpls.2020.00849.